

To be published in “Carbon-based magnetism: An overview of the magnetism of metal free carbon-based compounds and materials”, edited by T. Makarova and F. Palacio (Elsevier 2005)

Induced Magnetic Order by Ion Irradiation of Carbon-Based Structures

P. Esquinazi, R. Höhne, K.-H. Han,¹ D. Spemann, A. Setzer,
M. Diaconu, H. Schmidt, and T. Butz

*Institute for Experimental Physics II, University of Leipzig, Linnéstrasse 5, 04103
Leipzig, Germany*

Key words: Graphite, Magnetic properties, Irradiation effects, Disordered carbon, Fullerene

1 Motivation

Irradiation effects in graphite were one major research area in the past, partially due to its application as a moderator in thermal nuclear reactors. Graphite is still a material of choice for nuclear applications due to its low cross-section for neutron absorption. The influence of irradiation damage produced by different kinds of ions on several properties of graphite was reviewed by Kelly (1981) in chapter 7 of his book. Recently, irradiation effects in carbon nanostructures were reviewed by Banhart (1999). The effect of neutron irradiation

Email address: esquin@physik.uni-leipzig.de (P. Esquinazi).

¹ Present address: Department of Physics, Umeå University, Umeå, S-90735 Sweden.

on the magnetic properties of graphite has been studied in the past and shows the expected results, i.e. the introduction of lattice defects by irradiation produces a decrease in the diamagnetism and an increase in the spin density (Kelly, 1981). We are not aware of any study made in the past on the effects of proton irradiation on the magnetic properties of graphite or carbon-based structures.

When we started this research work on irradiation effects on the magnetism of graphite we had two reasons to choose protons as energetic particle. The first one is related to the analysis method called PIXE (Particle Induced X-ray Emission) that uses protons to get a map for all relevant impurity elements within a sample depth of 30 μm for a proton energy of ~ 2 MeV in carbon (see Sect. 2.2 for details). A systematic and full characterization of the magnetic impurity content in each of the samples, and after each treatment or handling (it makes no sense to start with a highly pure sample and then cut it with a steel knife afterwards), is of primary importance and absolutely necessary.

The second reason was based on early reports on room-temperature ferromagnetic behavior in some carbon-based structures (see references in Makarova (2003)). From those early works our attention was focused to the magnetic properties found in amorphous-like carbon prepared from different hydrogen-rich starting materials where an increase of the saturation magnetization with the hydrogen concentration in the starting material was found (Murata, Ushijima, Ueda, and Kawaguchi, 1991, 1992). The origin for the magnetic ordering has been related to the mixture of carbon atoms with sp^2 and sp^3 bonds, which was predicted to reach a magnetization higher than in pure Fe (Ovchinnikov and Shamovsky, 1991). Hydrogen, on the other hand, was assumed to have a role only in the formation of the amorphous carbon structure (Murata, Ushijima, Ueda, and Kawaguchi, 1992). New theoretical predictions, however, show that hydrogenated graphite can display spontaneous magnetization coming from different numbers of mono- and dihydrogenated carbon atoms (Kusakabe and Maruyama, 2003). Spontaneous magnetization may also appear in the case of monohydrogenated zigzag edges (Fujita, Wakabayashi, Nakada, and Kusakabe, 1996) if the distance between them is large or if they are not in parallel.

The advantage of proton irradiation is twofold: it enables us to make an impurity analysis simultaneously to the implantation of hydrogen. In this chapter we will review the main effects obtained after proton irradiation in different carbon-based structures. This chapter is organized as follows. In the next section we provide the main characteristics of our irradiation facility. In section 2.2 we show an example of element analysis obtained in one of the graphite samples used for the irradiation studies. The irradiation effects are reviewed in section 3. This section is divided in two main subsections that describe the effects in oriented graphite and carbon-based thin films. In section 4 we discuss some of the effects observed after annealing the sample at high temperatures

in vacuum or after leaving it at room temperature for a long period of time.

In this chapter we concentrate ourselves mainly on the effects produced by proton irradiation in highly oriented pyrolytic graphite (HOPG). Effects of irradiation with alpha particles will be discussed shortly in section 3.1.3. Iron and fluor irradiation effects on HOPG and on diamond are currently under way and the results will be published elsewhere in the future.

2 Irradiation Characteristics

All the irradiations presented in this chapter were done with the high-energy nanoprobe LIPSION of the University of Leipzig. The accelerator is a single ended 3 MV SINGLETRONTM with an RF-ion source for protons and alpha particles. The focusing system can deliver proton beams with diameters as low as 40 nm at very low currents of the order of 0.1 fA. For the present irradiations we worked at 2.25 MeV and currents up to 500 pA in the case of proton beam of diameter of 1 – 2 μm (microbeam). We have also irradiated samples with a broad beam of 0.8 mm diameter, energy of 2 MeV and currents between ~ 50 and ~ 150 nA. The X-ray detector is an Ortec HPGe IGLET-X and subtends 187 msrad solid angle. The numerical simulations discussed in this section are based on the code SRIM2003 (Ziegler, 1977-1985). The samples were mostly attached to a Si substrate using a small amount of Varnish or a mixture of Varnish with ultra-pure graphite powder. In one case we fixed the sample on a messing plate with a hole to enable the free penetration of the energetic particles (H^+ and He^+). The magnetic moment of the substrates was always measured before attaching the sample. All the irradiations were done at nominally room temperature; the temperature of the sample was not controlled during irradiation.

2.1 *The interaction of MeV-protons with graphite*

Figure 1(a) shows a typical profile for the number of defects created in a carbon matrix per 2.25 MeV-proton and per 1 μm interval. The penetration range of about 46 μm is clearly visible. For samples thicker than this range one expects that the majority of the protons will be stopped, whereas for samples substantially thinner essentially all protons traverse the sample. This means that for 20 μm or thinner samples the implantation of protons should be undetectable. Strikingly, enhancement of ferromagnetism has also been observed in disordered carbon (Höhne, Esquinazi, Han, Spemann, Setzer, Schaufuß, Riede, Butz, Streubel, and Hesse, 2004) and fullerene films deposited on Si substrates after proton irradiation (see section 3.2). Further details on the different processes that influence the

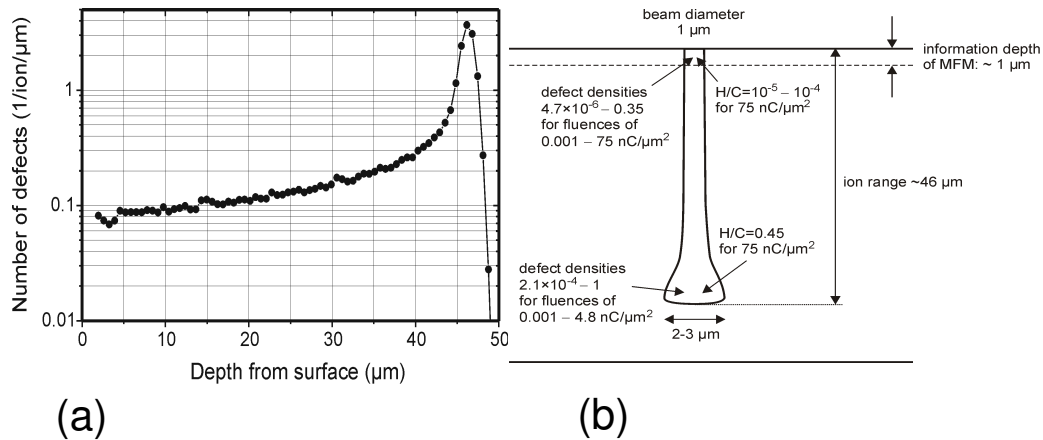


Fig. 1. SRIM2003 Monte Carlo simulations (Ziegler, 1977-1985) for 2.25 MeV protons on HOPG. (a) The number of defects per ion and 1 μm depth interval. The penetration range of 46 μm is clearly visible. (b) Sketch of the modified area in graphite due to 2.25 MeV proton bombardment. The lateral straggling has a full width at half maximum (FWHM) of $\sim 2.5 \mu\text{m}$ for an initial beam diameter of 1 μm . The numbers are obtained assuming a displacement energy of 35 eV for Frenkel pairs in HOPG. Adapted from Butz, Spemann, Han, Höhne, Setzer, and Esquinazi (2005).

penetration of protons in graphite as well as the restrictions of the SRIM2003 simulations were discussed by Butz, Spemann, Han, Höhne, Setzer, and Esquinazi (2005). The question how many protons remain in thinner samples cannot be clearly answered yet. Experiments with thinner and unsupported samples (to rule out part of the backscattering processes) are necessary and will be performed in the future. Under the assumption that there is no annealing of defects during irradiation and that the damaged area is of the same size as the irradiated one, the numerical simulations indicate that for fluences $0.001 \dots 75 \text{ nC}/\mu\text{m}^2$ we get in the near surface region between 4.7×10^{-6} and 0.35 displacements per carbon atom, i.e. complete amorphization for the highest fluence, using a displacement energy of 35 eV for Frenkel pairs in HOPG, in agreement with recently published studies of the damage cascades by irradiation on graphite (Abe, Naramoto, Iwase, and Kinoshita, 1997). Changing this number to 28 eV yields defect densities which are about 30% higher. Towards the end of the track, the lateral beam straggling becomes important and the damaged area can be several microns wide, see Fig. 1(b). For a fluence of $75 \text{ nC}/\mu\text{m}^2$ we have $\sim 5 \times 10^{11}$ protons/ μm^2 , i.e. the regions where defects are created by each individual proton overlap heavily.

Note that even for the highest fluence the relative concentration of hydrogen (H/C, see Fig. 1) in the first micrometer from the surface remains rather low, of the order of 10^{-4} or lower. However, most of what happens after the defect formation is still unclear. A dangling bond could attract a hydrogen atom - not necessarily from the proton implantation but already present as impurity in

the sample. Interestingly enough, there is little information on residual hydrogen from pyrolysis of hydrocarbons, possibly because detection methods for hydrogen contents of the order of 100 ppm or below were not readily available and such quantities were of little relevance for applications as moderators in reactors. Hydrogen atoms in the van der Waals gap or within the graphite layers should be highly mobile, contrary to hydrogen atoms trapped at defects. Investigations with deuterium done by Siegele, Roth, Scherzer, and Pennycook (1993) indicate that deuterium does not readily diffuse out of HOPG but is rather chemically bound up to D/C ratios of about 0.45, probably at lattice defects. The maximum retention of deuterium depends on the temperature and implantation energy. A broad range of binding energies for hydrogen in graphite up to about 4 eV was reported by Atsumi (2002), i.e. even temperatures as high as 3000-3500 K may be not sufficient to eliminate all incorporated hydrogen. On the other hand, the effective activation energies for hydrogen diffusion in our system are not necessarily the same as, for example, those obtained by experimental methods – usually at high temperatures – to study kinetics of diffusion of hydrogen in graphite. Irradiation effects of MeV protons on diamond-like films were studied by Wang, Wang, and Chen (1992). According to the authors, below a fluence of the order of $1 \text{ nC}/\mu\text{m}^2$ the hydrogen atoms produced by ion irradiation could be recaptured by dangling bonds. For higher fluences a release of hydrogen is expected.

Irradiation at a fixed energy has a clear disadvantage. If the magnetic ordering is triggered at a specific density of protons and defects, then, it is clear that with fixed proton and defect distributions, such as the one shown in Fig. 1, we would have a rather narrow window to get a maximum effect. Therefore, it should not be a surprise if for some irradiation energies and fluences one measures negligible effects or even a reduction of the magnetic order present in the sample before or after some irradiation steps. Carbon magnetism as well as irradiation effects on it belong to a new field in magnetism. For graphite bulk and thin film samples there are still many questions to be clarified in the future concerning the hydrogen implantation by irradiation and its effects on the magnetism.

The defect formation process by high energy protons is a non-equilibrium athermal process and it appears rather unlikely that ordered arrays of defects are formed by migration of interstitial carbon atoms or vacancies, maybe with the exception of the interstitial across the gallery. According to Banhart (1999) and from electron irradiation studies, the essential types of radiation damage up to intermediate temperatures are the rupture of basal planes (due to shift of the C-atoms out of the plane) and the aggregation of interstitials into small dislocation loops between the graphene layers. The migration energy of the interstitial depends whether it is bounded. Di-interstitials were proposed to explain the irradiation-induced amorphization of graphite with a migration energy of 0.86 eV (Niwase, 1995). The interstitial loops are stable up to rather

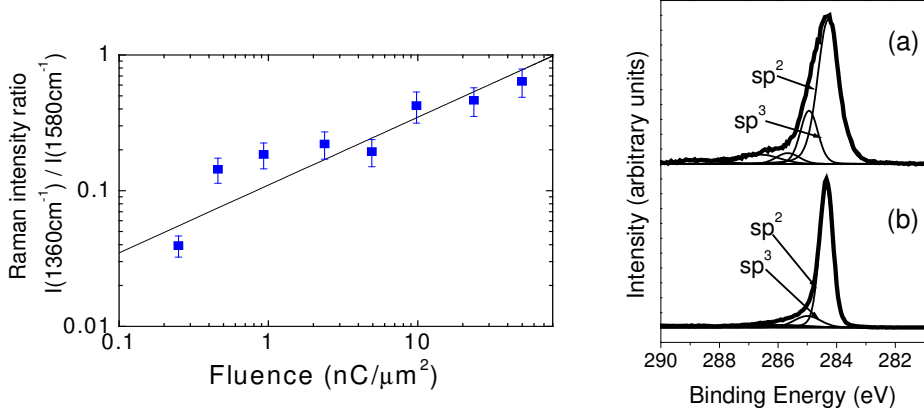


Fig. 2. Left figure: Raman intensity ratio as a function of the irradiation fluence for spots created on a HOPG sample (see section 3.1.2). The line represents the fit curve $0.1x^{0.5}$. Right figure: Decomposition of the XPS C_{1s} core-level peaks of HOPG surface after (a) and before proton irradiation (b). The components after peak fit are: at 284.4 eV: “C- sp^2 ”; at 285.0 eV: defect peak “C- sp^3 ”; other components: different C-O bonds. The thick and thin solid lines denote the experimental curves and the components, respectively. The measurement was done after irradiation of the sample with 1.2 mC and a fluence of $0.6 \text{ nC}/\text{mm}^2$ (step 4 of the sample reported by Esquinazi, Spemann, Höhne, Setzer, Han, and Butz (2003)). Adapted from Höhne, Esquinazi, Han, Spemann, Setzer, Schaufuß, Riede, Butz, Streubel, and Hesse (2004).

high temperatures, probably to 1000°C (Banhart, 1999). Certainly, the layer structure should remain essentially intact, at least for our low fluences and at the sample surface.

Irradiation can also produce a transition from sp^2 to sp^3 bonding leading to cross-links between the graphene layers and the formation of sp^3 clusters (Tanabe, 1996). These clusters appear to be stable and do not anneal at high temperatures. Our own Raman and X-ray Photoemission Spectroscopy (XPS) measurements indicate the following. For all unirradiated areas of the HOPG samples the Raman spectra show only one pronounced peak at 1580 cm^{-1} (the E_{2g_2} mode) as expected for graphite without any disorder. For the spots produced with the proton microbeam the Raman spectra show additionally the disorder mode D at 1360 cm^{-1} . With increasing fluence the E_{2g_2} and D modes become broader and the ratio of their intensities $I(\text{D})/I(\text{E}_{2g_2})$, as a measure of the degree of disorder, increases (see Fig. 2).

The XPS results show a clear difference between an irradiated and an unirradiated sample, see Fig. 2. The C_{1s} core-level peaks of HOPG samples were recorded using a pass energy of 10 eV and were fitted by six components with binding energies of 284.4 eV (main peak of HOPG, C- sp^2), 285.0 eV (defect peak “C- sp^3 ”), 285.8 eV, 286.3 eV, 289.0 eV (C-O components) and 290.9 eV (shake-up peak). The main result is that the defect peak component increases

after proton irradiation. A similar behaviour was found for HOPG under plasma low-energy argon-ion bombardment (Rousseau, Estrade-Szwarczopf, Thomann, and Brault, 2003). Whether this defect peak corresponds to a pure C-sp³ state or whether some of the “defect” carbon atoms are bounded to hydrogen is unclear and it is a matter of current research (Estrade-Szwarczopf, 2004). The knowledge of the C-H sp² and sp³ bonds is for the magnetic properties of carbon structures of importance. We remark that numerical simulations indicate a 100% polarized π -band, i.e. a ferromagnetic order stable at room temperature, for a graphene layer with a mixture of sp² and sp³ bondings (mono- and di-hydrogenated) at the zigzag edges of a graphene layer (Kusakabe and Maruyama, 2003).

Other aspect of the irradiation effects on graphite that may be of importance to trigger magnetic ordering is the formation of pentagons and heptagons in the basal planes, which could cause a bending of the graphene layers (Banhart, 1999). The influence on the electronic band structure of graphite of such topological defects has been studied theoretically by González, Guinea, and Vozmediano (2001). According to these authors, these defects may trigger ferromagnetism or even superconductivity.

For thick targets and sufficiently high fluences, the target surface actually swells, which can be easily measured by an atomic force microscope (AFM), see Fig. 8(a), or is even visible under an optical microscope (Spemann, Han, Esquinazi, Höhne, and Butz, 2004; Esquinazi, Han, Höhne, Spemann, Setzer, and Butz, 2005). The swelling in the c -direction occurs together with the contraction in the graphene layer; the new formed interstitial planes push the existing planes apart leading to a protuberance at the sample surface. This irradiation effect was studied by Koike and Pedraza (1994); Muto and Tanabe (1997); Takeuchi, Muto, Tanabe, Arai, and Kuroyanagi (1997). This effect was not observed for thin enough targets for the usual proton irradiation fluences used in this work.

Another important aspect regarding the irradiation effects is the heat load due to the beam. For a spot of $2\ \mu\text{m} \times 2\ \mu\text{m}$ and a current of 500 pA this amounts to $\sim 300\ \text{W}/\text{mm}^2$ for thick samples. Most of the energy will be deposited near the end of the ion track. Depending on the lateral dimensions and the thickness of the sample as well as the target holder, heat is transported away from the beam spot. The details are difficult to calculate, but the measurement and control of the temperature is of importance. For thin samples, this is relatively unimportant. We have evidence that at higher currents the magnetic response in MFM-measurements is strongest at the rim of the spot suggesting annealing effects in the center of the spot, as Fig. 3 indicates. For lower currents the magnetic image is homogeneously distributed across the spot (see section 3.1), in contrast to the magnetic “ring” shown in Fig. 3.

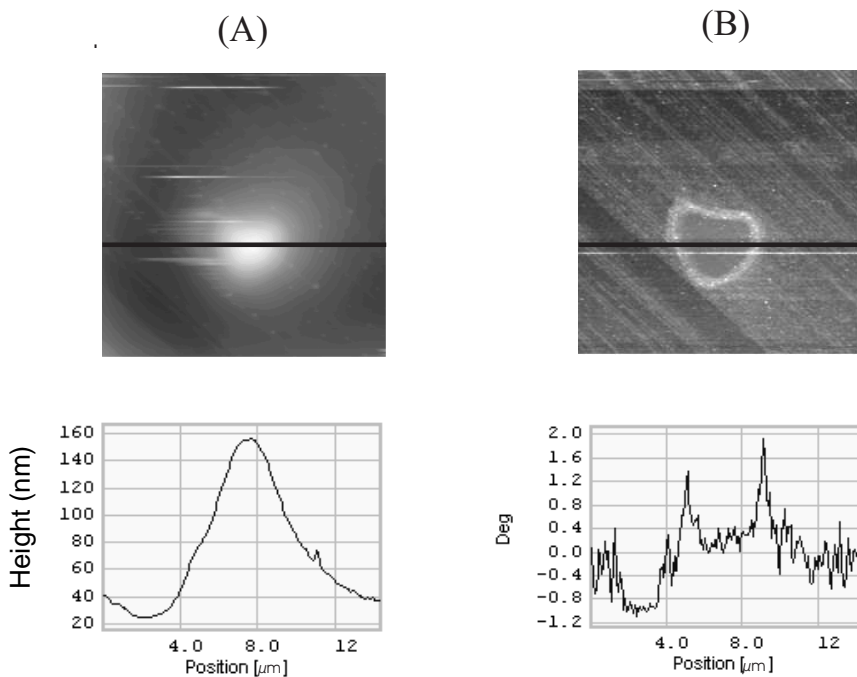


Fig. 3. (A) Topography and (B) MFM images obtained from a spot produced with a dose of $6.8 \text{ nC}/\mu\text{m}^2$ and a current $I = 0.51 \text{ nA}$, which means a current density larger than $5 \text{ mA}/\text{cm}^2$. The scan area is $15 \mu\text{m} \times 15 \mu\text{m}$. The bottom figures show the line scans done at the positions of the black lines of the upper pictures. The MFM images were taken at a distance of 50 nm using standard magnetic tips. Taken from Esquinazi, Han, Höhne, Spemann, Setzer, and Butz (2005)

2.2 Impurity measurements

With the proton micro-beam a total charge of $0.5 \mu\text{C}$ suffices to obtain a minimum detection limit for Fe impurities below $1 \mu\text{g}/\text{g}$. With our broad-beam PIXE facility we work with 2 MeV protons and currents of 150 nA and a beam diameter of 0.8 mm . Here, about $5 \mu\text{C}$ are required to reach a minimum detection limit of $1 \mu\text{g}/\text{g}$ for Fe. The fluences are in the range of $1 \dots 50 \mu\text{C}/\text{mm}^2$ for the micro-beam and the broad-beam, respectively. These fluences are several orders of magnitude lower than the fluences actually applied for the induction of magnetic ordering in graphite, as will be discussed below. The advantage of the micro-beam compared to the broad-beam is that a distribution map for all relevant impurity elements can be obtained contrary to the integral value for the broad-beam method, a rather important issue considering the grossly inhomogeneous distribution of impurities like Fe which we have encountered in some samples (see for example Fig. 1 in Spemann, Han, Höhne, Makarova, Esquinazi, and Butz (2003)). A typical broad beam PIXE spectrum for a HOPG sample is shown in Fig. 4. It shows the presence of a number of impurities, the Fe content being $(0.45 \pm$

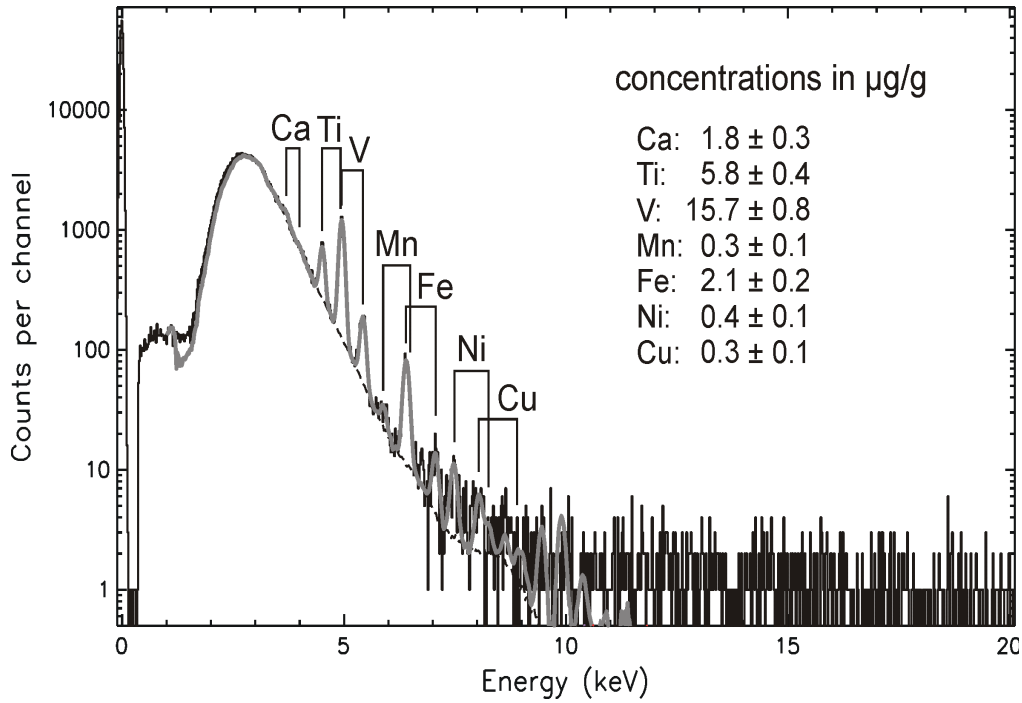


Fig. 4. Typical broad beam PIXE spectrum from a HOPG sample. The main impurities are Ti, V, and Fe. The minimum detection limit for other elements heavier than Si is $\sim 0.3 \mu\text{g/g}$. Note that $2.1 \mu\text{g/g}$ iron in the carbon matrix means a concentration of 0.45 ppm Fe. The background curve is due to the carbon matrix.

0.04) ppm. From the study of ferromagnetic signals in different HOPG samples (Esquinazi, Setzer, Höhne, Semmelhack, Kopelevich, Spemann, Butz, Kohlstrunk, and Lösche, 2002) we may suspect that HOPG could contain a non negligible amount of hydrogen, some of them may be related to the origin of the magnetic signals. The amount of hydrogen before or after irradiation within the fluence used in this work cannot be determined by PIXE. Taking into account recently done theoretical work done by Lehtinen, Foster, Ma, Krasheninnikov, and Nieminen (2004) that estimates a magnetic moment of $\sim 1 \mu_B$ for a carbon vacancy, $2.3 \mu_B$ in the surrounding of an hydrogen bonded to a carbon atom at the position of a carbon vacancy, or $1.2 \mu_B$ for a vacancy that is saturated by two hydrogen atoms in a graphene layer, we may expect that a few ppm hydrogen trigger a non negligible magnetic signal in graphite. Therefore, hydrogen content measurements should be carried out with a sensitivity in the ppm range, a rather difficult task. The reader can read Butz, Spemann, Han, Höhne, Setzer, and Esquinazi (2005) for a short discussion on the methods available for this kind of measurement.

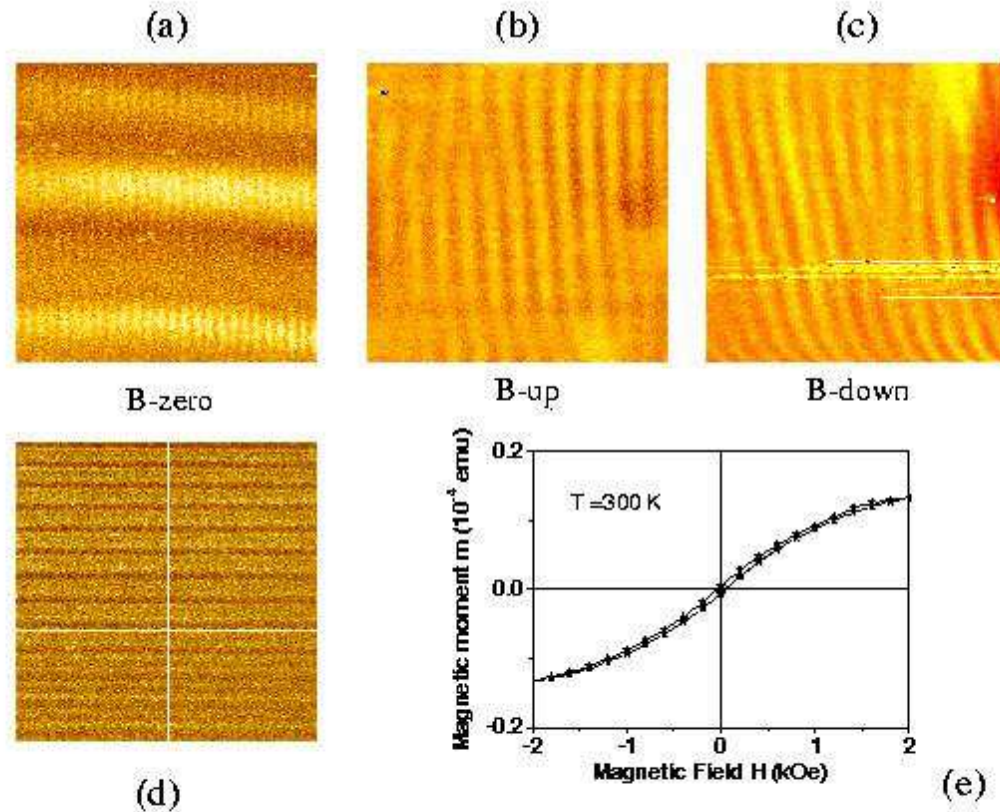


Fig. 5. Magnetic force microscope (MFM) and SQUID measurements of a HOPG sample irradiated with 4 broad spots ($\phi \simeq 0.8$ mm) of $135 \mu\text{C}$ total charge each. All images scan an area of $20 \times 20 \mu\text{m}^2$: (a) MFM image of the sample in the state just after irradiation, (b) after application of a field of $+1$ kOe, (c) after application of a field of -1 kOe. All measurements were done in remanent state after removing the field, i.e. at no applied field. (d) Magnetic domain structure of the sample in the same state as in (a) but at a different position. All the MFM measurements were done with a standard magnetized MESP tip and at a distance of 50 nm from the sample surface. (e) The magnetic moment of the same sample measured with a SQUID at room temperature. The sample was fixed on a Si substrate for the irradiation. The data in the figure are the original data of the sample with Si substrate, without any subtraction. The signal of the sample overwhelms that from the substrate. Measurements of the sample standing alone reproduces basically the curve presented here.

3 Irradiation Effects

3.1 On highly oriented pyrolytic graphite

3.1.1 Broad proton irradiation

All the irradiated HOPG samples discussed in this review were from Advanced Ceramics Co. (ZYA grade, 0.4° rocking curve width at half maximum) with a content of magnetic metallic impurities below 1 ppm. The largest concentration of non magnetic metallic ions was found for Ti ($\lesssim 6 \mu\text{g/g}$) and V ($\lesssim 16 \mu\text{g/g}$). A typical surface area of the samples was $2 \times 2 \text{ mm}^2$ and a thickness between 0.1 mm to 0.3 mm. The samples were glued with varnish (or a mixture of varnish and a high purity graphite powder to increase the thermal coupling) on a high-purity Si substrate and the magnetic moment of the whole ensemble as well as of the Si substrate alone was measured. In general and within experimental error the diamagnetic hysteresis loops for the used Si substrates are reversible; after subtracting the linear diamagnetic dependence there is no significant hysteresis left (for an example see Fig. 7(a)). Nevertheless, when the ferromagnetic moment of the sample is weak, it can be a hard task to obtain the true sample magnetic moment from the SQUID signal of the mixture (Si plus the HOPG sample) and several checks have to be done.

In this section we will discuss results obtained after irradiation of a large area of the HOPG sample using the micro- and the broad-beam of protons. As we will realize below, there are several irradiation parameters that may have an important role in inducing the achieved magnetic signal. Namely:

- (1) The total implanted charge. The total amount of protons or alpha particles that were implanted in the sample or travelled through the sample.
- (2) The input energy. Although with the LIPSION we have the possibility of changing this energy from 1 to 2.25 MeV, in order to minimize the number of variables, the studies presented here were done with fixed irradiation energies of 2.0 or 2.25 MeV. This means that we have a well defined defect and implantation profile inside the sample, see Fig. 1. If the highest magnetic signal is determined at a given defect and proton density, it is clear that successive irradiation at similar energies may produce contrary effects if this optimized region is destroyed by the next irradiation at similar conditions.
- (3) The fluence, the irradiated charge per unit area.
- (4) The ion current. Large currents might heat the sample and non systematic effects are then possible.
- (5) Micro- or macro-irradiation, i.e. a broad irradiation with the 0.8 mm beam or a large number of micrometer spots distributed in the sample. Experience indicates that the magnetic signals are much larger when one uses a high density of micrometer spots rather than the implantation of similar amount of charge with a broad beam. This fact appears to be related with the

density and/or type of defects that the beam produces.

– (6) Sample temperature. All the irradiations presented in this review were done at nominally room temperature. Future experiments should try to irradiate at lower or higher temperatures to check for its influence.

– (7) Finally, the initial state of the sample, namely the density and type of defects, which in part can determine its metallicity. Computer simulation results of the effects of adsorbed hydrogen on the band structure of a graphene layer indicate that metallization caused by specific defects can quench a spin polarized state (Duplock, Scheffler, and Lindan, 2004).

The first SQUID measurements that indicate a magnetic ordering after proton irradiation were published by Esquinazi, Spemann, Höhne, Setzer, Han, and Butz (2003). In that work an increase in the hysteresis loop was observed after several irradiation steps. These irradiation steps contained successively irradiation of several thousands of micrometer small spots as well as four (or three) spots of 0.8 mm diameter each on the same sample. In what follows we shall discuss further work that has been done afterwards, where we have tried to characterize the effects produced by some of the irradiation parameters described above. We stress that they are the very first steps to get reproducible magnetic order in carbon, a task that turned to be full of difficulties, as the published results from literature indicate.

A broad and homogeneous proton irradiation of usual fluences ($\sim 150 \mu\text{C}$ total charge in an area of $\sim 1 \text{ mm}^2$) per spot on oriented graphite produces a magnetic signal that in general can be well observed with a magnetic force microscope (MFM) on the irradiated surface. Figure 5 shows the MFM images obtained on an irradiated area with a total charge of $540 \mu\text{C}$ distributed into 4 spots, $135 \mu\text{C}$ each. After this broad irradiation there is no significant change in the topography worth to note. However, the periodic magnetic domains are well defined. In the remanent state just after irradiation, in some of the irradiated area of the sample we observed two domain structures, one normal to the other, see Fig. 5(a). The period of the small domain structure is $\sim 0.8 \dots 1.2 \mu\text{m}$ depending on the region (compare with (d) which was obtained in the same state but in other irradiated area), whereas the other domain structure has a period of $\sim 10 \mu\text{m}$ and depends on the scan direction of the MFM tip. After application of a field of 1 kOe in the $+z$ direction (perpendicular to the graphene layers) the “vertical” domain structure shows a period of $\sim 1.6 \dots 2.0 \mu\text{m}$ and the width of the domains increases, see Fig. 5(b). The other domain structure is not observed. After magnetizing the sample with a field in the other direction there is a slight change of the width of the bright relative to the dark regions, compare (c) with (b). In non-irradiated graphite areas we did not find any signature of domain structures within the resolution of the microscope. This irradiation triggered a relatively large hysteresis loop that could be very well measured with the SQUID without any background subtraction, see Fig. 5(e). The temperature dependence of this signal was

studied removing the sample from the Si substrate. It shows a weak decrease ($\sim 5\%$) with temperature of the saturation magnetization and coercivity fields between 5 K and 300 K.

To study the influence of some of the irradiation parameters on the magnetic response of HOPG samples, we have studied three HOPG samples from the same batch. One sample of mass $m = 1.19$ mg (labelled AS171103/2) was irradiated with the proton microbeam as follows. First irradiation consisted of 10^4 spots of diameter $\phi \simeq 1.8$ μm each with a charge of 0.85 nC (total charge 8.5 μC), fluence = 0.34 nC/ μm^2 , irradiated area: 0.62×0.62 mm^2 and current $I \simeq 1.1$ nA. Second irradiation produced the same amount of spots but with a diameter of $\phi \simeq 2$ μm and 0.72 nC charge each (total charge 7.2 μC), fluence = 0.24 nC/ μm^2 and $I \simeq 0.9$ nA. The third and last irradiation was identical to the first one. The room temperature SQUID results of the sample before and after subtraction of the diamagnetic background are shown in Fig. 6. It is clearly seen that the irradiation increases the magnetic signal of the sample. The last irradiation, however, did not produce any significant change respect to the last one. The remanent magnetization changed from $M_r(B = 0) \simeq 3.3 \times 10^{-5}$ emu/g to 2.7×10^{-4} emu/g and 4.5×10^{-4} emu/g for the first, virgin state and second (or third) irradiation steps.

To check the influence of the irradiation current under broad irradiation conditions we have irradiated two samples with the following characteristics. Irradiation with a current $I = 54 \pm 1$ nA: sample AS211003/1, mass $m = 1.33$ mg, first irradiation: 4 spots of $\phi = 0.8$ mm and 53.4 μC each (total charge 214 μC); second irradiation: 4 spots of $\phi = 0.8$ mm and 110 μC each (total charge 440 μC); third irradiation: 4 spots of $\phi = 0.8$ mm and 54.5 μC each (total charge 218 μC). The SQUID results after subtraction of the diamagnetic background are shown in Fig. 7(a). We see that the initial magnetic state of this sample (magnetic moment at saturation $m \simeq 10^{-6}$ emu) decreased after the first irradiation. For the subsequent irradiation steps the magnetic moment increased. The saturation magnetization showed a decrease from its initial value of $M_r = (1.95 \pm 0.15)10^{-4}$ emu/g to $M_r = (1.0 \pm 0.08)10^{-4}$ emu/g after the first irradiation. For the 2nd and 3rd irradiation we have $M_r = (1.56 \pm 0.15)10^{-4}$ emu/g and $M_r = (2.6 \pm 0.15)10^{-4}$ emu/g. The coercive field remains in the range of 150 Oe.

On the sample AS181103 of mass $m = 1.12$ mg, the following irradiation steps at a proton current of $I = 150$ nA were performed: (1) 2 spots of 0.8 mm diameter with 159 μC each (total charge 318 μC); (2) 2 spots of 0.8 mm diameter with 160 μC each (total charge 320 μC); (3) 2 spots of 0.8 mm diameter with 154 μC each (total charge 308 μC). Figure 7(b) shows the SQUID results for this sample. Under those irradiation conditions the sample did not show any significant increase in the magnetic signal within experimental error. Comparing this result with that of (a) we would conclude that the proton current

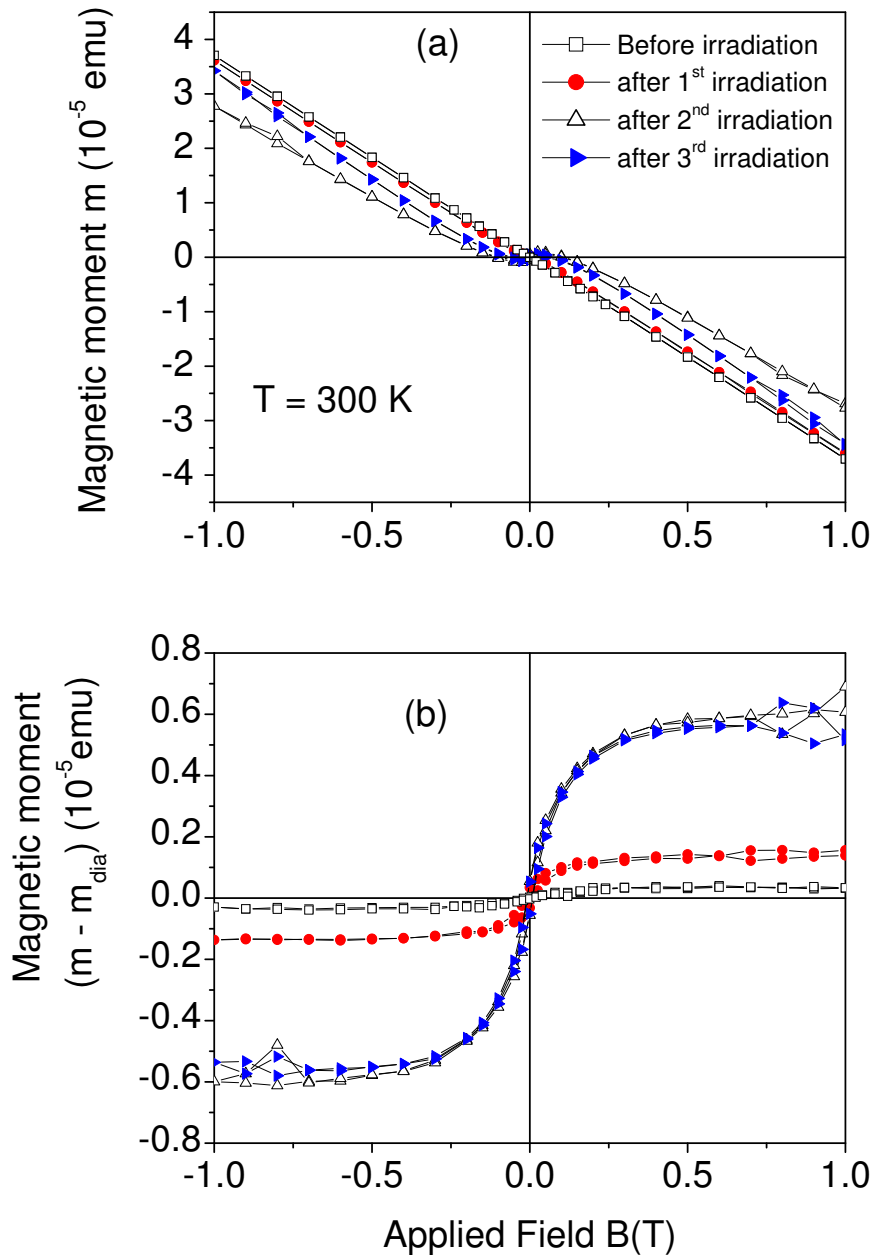


Fig. 6. (a) Magnetic moment vs. applied field of the HOPG sample AS171103/2 glued on a Si substrate before and after irradiation (for details see text). (b) The same data as (a) but after subtraction of the diamagnetic background.

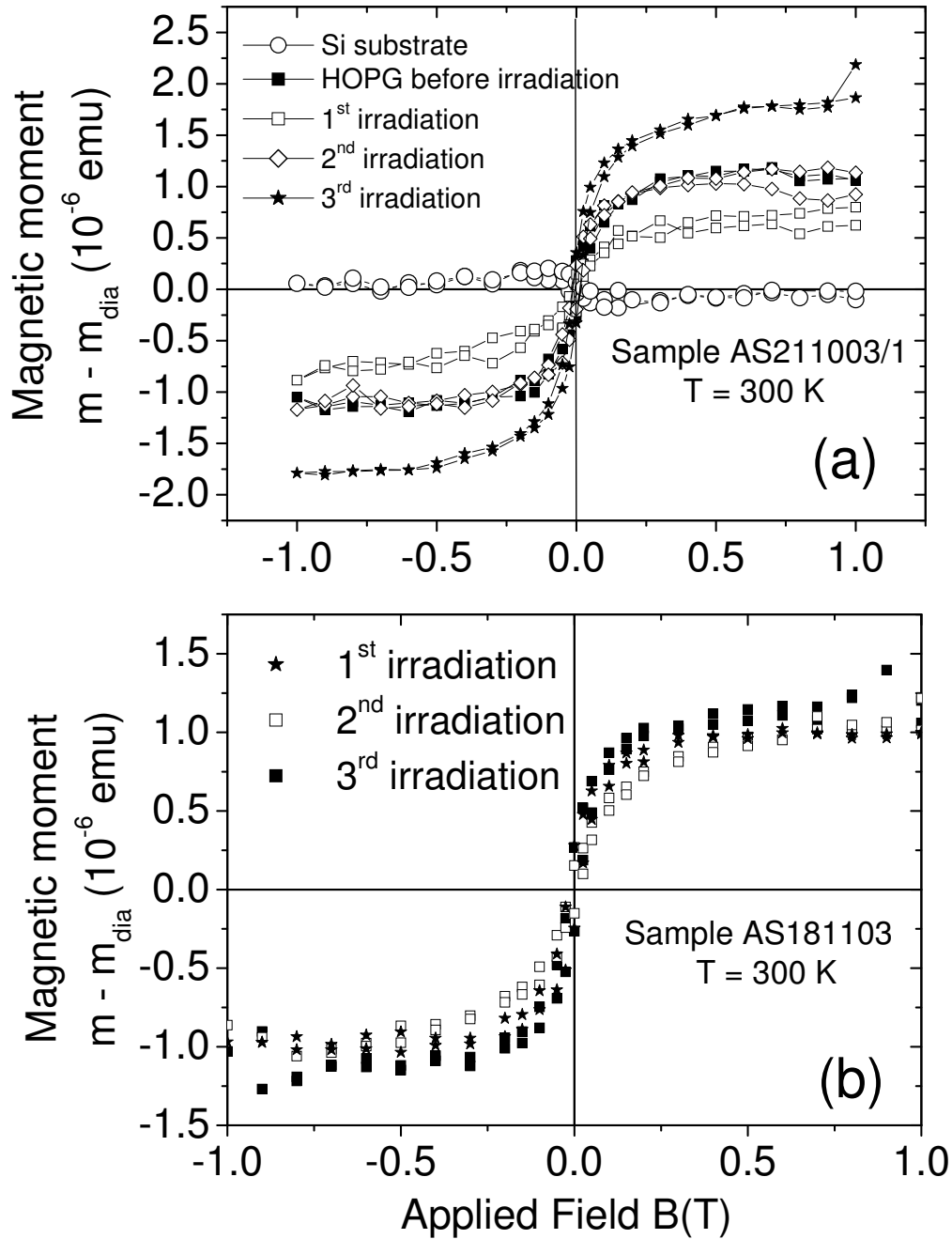


Fig. 7. (a) Magnetic moment (minus the diamagnetic background) vs. field of a typical Si substrate (\circ) where all HOPG samples were attached before and after all irradiation steps. The other symbols correspond to sample AS211003/1 after different proton irradiations (see text for details) with proton current $I \sim 55$ nA. (b) The same for sample AS181103 after different proton irradiations with a current $I \simeq 150$ nA (for details see text).

plays an important role in inducing the magnetic ordering in HOPG samples.

3.1.2 *Magnetic spots and lines of micrometer size*

As mentioned in section 2, the LIPSION accelerator has the possibility to irradiate the samples with a proton micro- or nanobeam. We have used the microbeam to produce magnetic spots on oriented graphite surfaces. As for the broad beam irradiation, the microbeam was directed onto the HOPG surface parallel to the c -axis of the sample without beam scanning (excepting line scans, see below) leading to the formation of micron-sized spots with enhanced defect density, as measured by micro-Raman, see Fig. 2. In general, two spots separated by a distance of $20\ \mu\text{m}$ were irradiated with the same ion fluence and several ion fluences were used. For large enough fluences the swelling at the spots can be directly observed with an optical microscope (Spemann, Han, Esquinazi, Höhne, and Butz, 2004; Esquinazi, Han, Höhne, Spemann, Setzer, and Butz, 2005). The height of this swelling depends on the irradiated fluence and on the mass of the ions. The dependence of the maximum swelling height, measured by AFM, with the fluence for proton irradiation is shown in Fig. 8(a). With a MFM one can measure the magnetic signal on the spots. The maximum amplitude of the signal (maximum phase shift) as a function of the fluence for two different proton currents is presented in Fig. 8(b). The units of the magnetic signal from the MFM are “degrees”; a relation of this phase shift of the tip vibration to the force gradient can be found in Lohau, Kirsch, Carl, Dumpich, and Wassermann (1999); Lohau, Kirsch, Carl, and Wassermann (2000). Examples for the magnetic moment calculated from measurements of the phase shift in carbon samples can be found in Han, Spemann, Höhne, Setzer, Makarova, Esquinazi, and Butz (2003b,c); Han and Esquinazi (2004).

We note that, whereas the swelling height increases systematically with fluence, the maximum phase shift of the magnetic signal does not, see Fig. 8(b). This result indicates that: (1) there is a negligible influence of the topography onto the magnetic signal and (2) the magnetic signal depends on the implanted charge, proton current and probably also on the carbon structure. The difference between the behaviors observed for two different proton currents can be understood if we take into account that the higher the current the higher would be the internal temperature of the sample at the spot. Therefore, annealing effects can be the origin for this difference. It is worth to note that the signals could be reproduced after leaving the samples in air and at room temperature for two months, see Fig. 8(b). This is not the case for much larger times, see section 4. We note also that at the higher fluence range, the structure of the spots is very probably that of highly disordered or even amorphous carbon. For both proton currents the maximum magnetic signal decreases at the highest fluences, see Fig. 8(b).

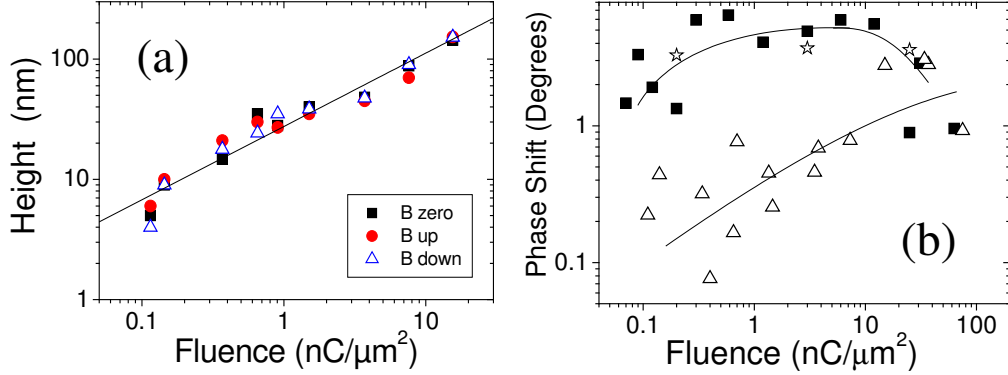


Fig. 8. (a) Maximum height of swelling as a function of the fluence, measured at micrometer small spots with an AFM. The three symbols indicate the height measured before and after the application of a magnetic field in z (up) and $-z$ (down) direction. The measurements were done without applied field. The line is the function $27.5x^{0.61}$ nm with x being the fluence in $\text{nC}/\mu\text{m}^2$. (b) Maximum phase shift measured at micrometer small spots on two different HOPG samples, before application of a magnetic field, as a function of the irradiation fluence. The spot areas were $1 \mu\text{m}^2$ (■, ★) and $4 \mu\text{m}^2$ (△); the corresponding proton currents were 171 pA and 855 pA, respectively. The (★) symbols correspond to the same sample measured again two months later. The lines are only a guide to the eye.

Figure 9 shows an example of a magnetic spot as measured with the MFM before and after application of a magnetic field in two directions. The irradiated region can be clearly recognized as the “white” spot of the magnetic images in (a). A line scan through these images indicates clear changes of the phase shift after application of a magnetic field, see top figure in Fig. 9(b). Usually the magnetic images are obtained with a tip to sample distance of 50 nm. If we increase this distance the phase shift amplitude decreases. This dependence can be used to estimate, although with a relatively large error, the order of magnitude of the magnetization at the spot surface. From the data shown in the bottom figure of Fig. 9(b) one is able to estimate a magnetization of the order of 400 emu/g (Han and Esquinazi, 2004), a very large magnetization of the order of soft ferromagnetic metals.

As a first attempt to write magnetically on a graphite surface we have started with a simple cross. Figure 10(a-c) shows the magnetic images for two crosses made at different irradiation fluences and measured with different tips and the topography for one of them (d). The magnetic image changes after applying a magnetic field. The results after magnetizing the cross show a state with one or three magnetic domains. Micromagnetic simulations with the appropriate parameters provide similar MFM images (Schindler, Spemann, Ziese, Diaconu, Schmidt, Esquinazi, and 2005) and they may be used to obtain material parameters (magnetic anisotropy, for example) that are not yet possible to measure directly.

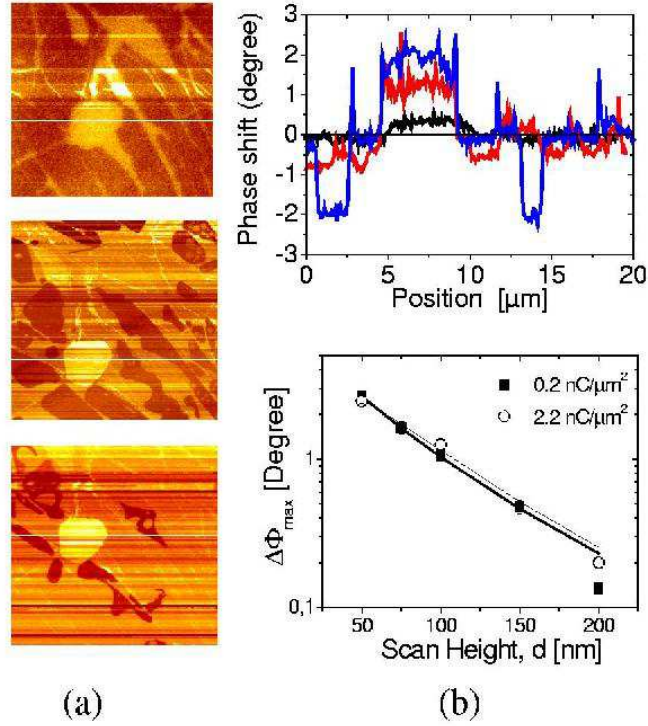


Fig. 9. (a) Magnetic force gradient images ($20 \times 20 \mu\text{m}^2$) of a spot and its surroundings irradiated with $0.115 \text{ nC}/\mu\text{m}^2$ (proton current $I = 171 \text{ pA}$). The images were taken, from top to bottom, before field application, after applying a field of $\sim 1 \text{ kOe}$ in the $+z$ direction parallel to the c -axis, and in the $-z$ direction. The tip-to-sample distance was 50 nm . (b) Top: The corresponding phase shift obtained at the line scans (white straight lines in figures (a)). The spot is located between $\sim 5 \mu\text{m}$ and $\sim 10 \mu\text{m}$. The bottom, upper and middle lines in this region correspond to measurements before and after application of a field in $-z$ and $+z$ direction. Adapted from Han, Spemann, Esquinazi, Höhne, Riede, and Butz (2003a). Bottom: Scanning height dependence of the maximum phase shift at proton irradiated spots with fluences of $0.2 \text{ nC}/\mu\text{m}^2$ and $2.2 \text{ nC}/\mu\text{m}^2$. Solid lines are fits with the point probe approximations. Adapted from Han and Esquinazi (2004).

3.1.3 Irradiation effects with alpha particles

With the LIPSION accelerator we have also the possibility to irradiate the samples with a microbeam of 1.5 MeV alpha (He^+) particles. The SRIM2003 simulation indicates that the penetration depth of these particles in graphite should be $4 \mu\text{m}$. For a fluence of $0.1 \text{ nC}/\mu\text{m}^2$ the defect density at the surface should be 1.4% and the region at the end of ion range should be rather amorphous. As for protons, we have produced pairs of spots at different fluences and studied the magnetic signal at the spot position with MFM. Figure 11 shows the topography and magnetic images and the line scans of a spot produced with a fluence of $0.1 \text{ nC}/\mu\text{m}^2$. Whereas the swelling produced by

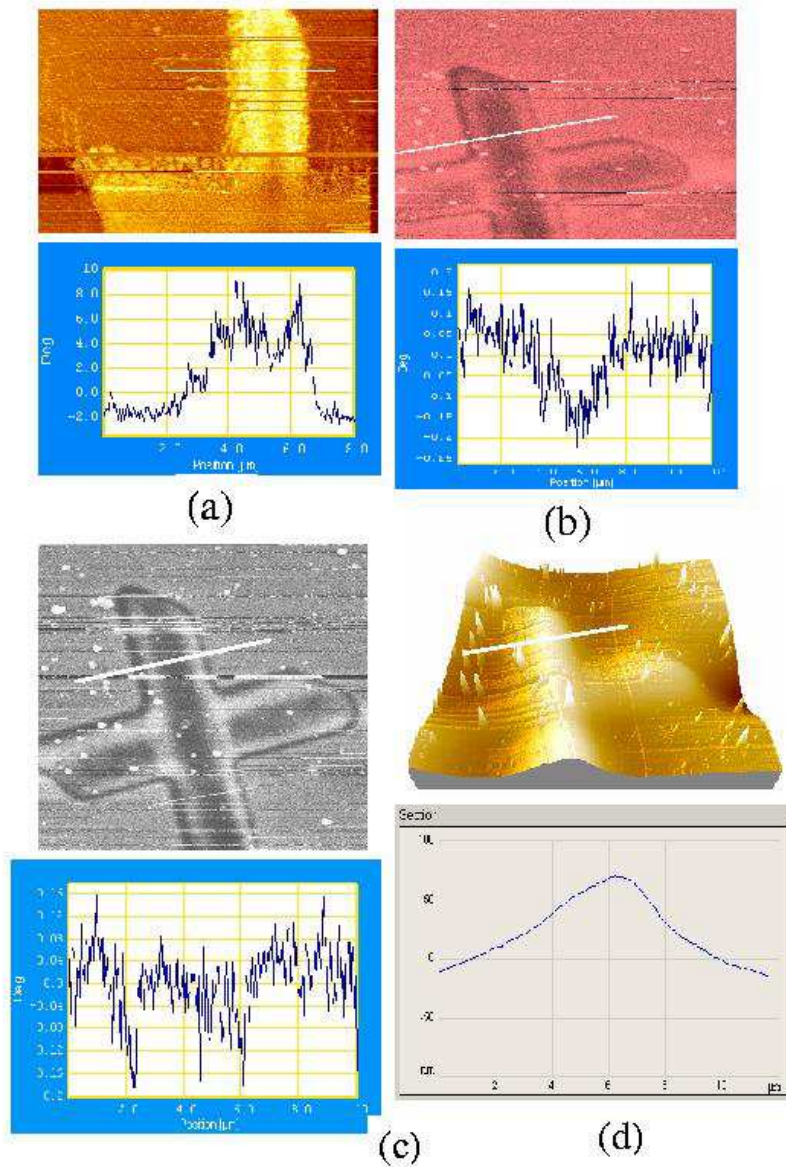


Fig. 10. (a) Magnetic image (top, $8 \times 16 \mu\text{m}^2$) and the corresponding phase shift (bottom) obtained at the line scan (white lines in all figures) for a cross produced with a fluence of $0.5 \text{ nC}/\mu\text{m}^2$ and a proton current of $I = 120 \text{ pA}$. The measurement was done before applying any magnetic field and with a LM (low moment), well magnetized tip. (b) Similar to (a) but for a cross produced with a fluence of $2 \text{ nC}/\mu\text{m}^2$ and after application of a field of 1 kOe normal to the surface. The magnetic image has a size of $18 \times 18 \mu\text{m}^2$ and was taken with a standard MESP tip. (c) The same cross as in (b) but after application of a field of 2 kOe in the same direction as in (b). The magnetic image has a size of $10 \times 20 \mu\text{m}^2$. (d) Three dimensional image of the topography of the cross in (b,c) and the corresponding line scan (bottom).

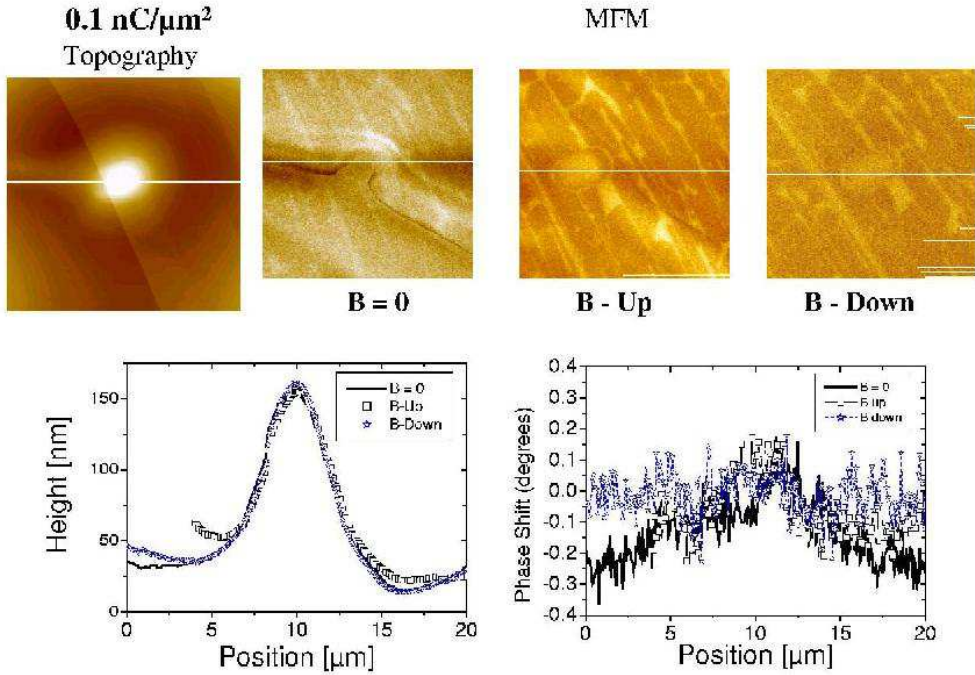


Fig. 11. Micrometer spot produced after irradiation of alpha particles of 1.5 MeV on a HOPG surface with a fluence of $0.1 \text{ nC}/\mu\text{m}^2$. The upper pictures show the topography (left) and the magnetic images before application of a magnetic field ($B=0$), and after the application of a field in $+z$ (B -up) and in $-z$ direction (B -down). The bottom pictures show the line scans obtained at the position of the white lines in the upper images.

the He^+ irradiation is remarkable, we recognize that the maximum phase shift measured by the MFM at the spot and its surroundings, see Fig. 11, is much smaller than those obtained at the spots produced with protons, see Fig. 9. Nevertheless, the fact that we can measure small but not zero signals, indicates that ion-, other than proton-, irradiation in the carbon structure may also trigger magnetic ordering. As we mentioned above, we do not know yet whether the hydrogen already present in the sample before irradiation or in the irradiation environment (rest gases in the chamber, for example) plays any role and therefore we should take these results with caution as a proof for a hydrogen-independent magnetic ordering. Future work should try to measure HOPG samples irradiated with alpha particles at different fluences and with the SQUID.

3.2 On thin films

Taking into account the irradiation profile of protons in carbon obtained from Monte Carlo simulations, see Fig. 1, one would expect no or negligible effects

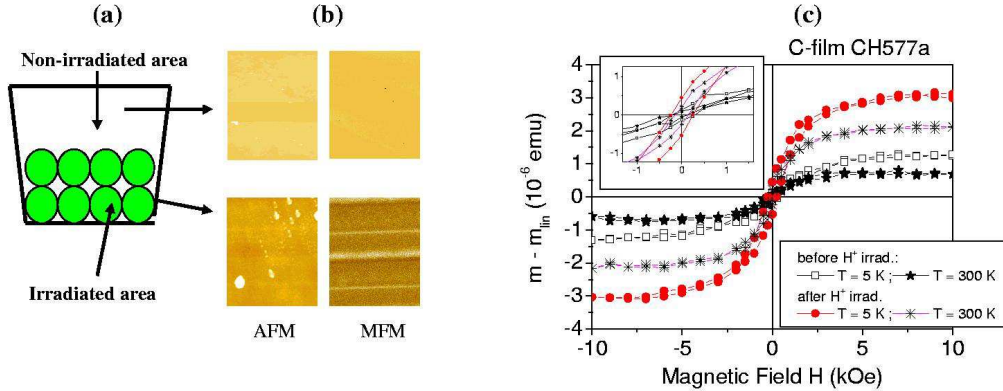


Fig. 12. (a) Sketch of the disordered carbon film CH577a produced by pulsed laser deposition with the irradiated (8 spots with 0.8 mm diameter and 150 μC total charge each) and non-irradiated areas. (b) Topography (AFM) and magnetic (MFM) images in both areas. (c) Magnetic moment of the film (after subtraction of the linear diamagnetic background) as a function of magnetic field applied parallel to the main area. The symbols (\square, \star) indicate: before irradiation, measurements done at $T = 5$ K and 300 K, and after proton irradiation, (\bullet, \ast) at 5 K and 300 K. The inset shows an enhanced part around zero field. Adapted from Hohne, Esquinazi, Han, Spemann, Setzer, Schaufu, Riede, Butz, Streubel, and Hesse (2004).

on the magnetic properties of samples, which thickness is much less than ~ 40 μm , because most of the protons would go through the sample leaving a small density of defects. We have checked this assumption irradiating carbon and fullerene films with thickness below 1 μm . Figure 12 shows the MFM and SQUID results of a carbon film produced by pulsed laser deposition (PLD) in a hydrogen (H_2) atmosphere and deposited on a Si substrate. On the film 8 spots of 0.8 mm diameter were irradiated (see sketch in the figure). The MFM signal shows magnetic domains in the irradiated region only, see Fig. 12(b). The SQUID shows a clear increase in the magnetic moment after irradiation, see Fig. 12(c). Because the results are taken on an disordered sample, they also reveal that a graphite ordered structure, at least in the mesoscopic level, is not necessary to trigger magnetic order after irradiation.

Makarova, Han, Esquinazi, da Silva, Kopelevich, Zakharova, and Sundqvist (2003) studied the magnetism in photopolymerized fullerene films by MFM. The magnetic force gradient measurements revealed that laser- and electron-beam irradiation of fullerene films produces magnetic images highly correlated to the topography. This correlation is expected since the polymerization shrinks the film material at the surface within a certain penetration depth, which depends on the radiation characteristics, producing topographic clusters with magnetic order. An example of the AFM and MFM images in a region illuminated in air with an energy of 2.6 eV and intensity of 200 mW/cm^2 is shown in Fig. 13. The high correlation between of magnetic grain formation and topography is

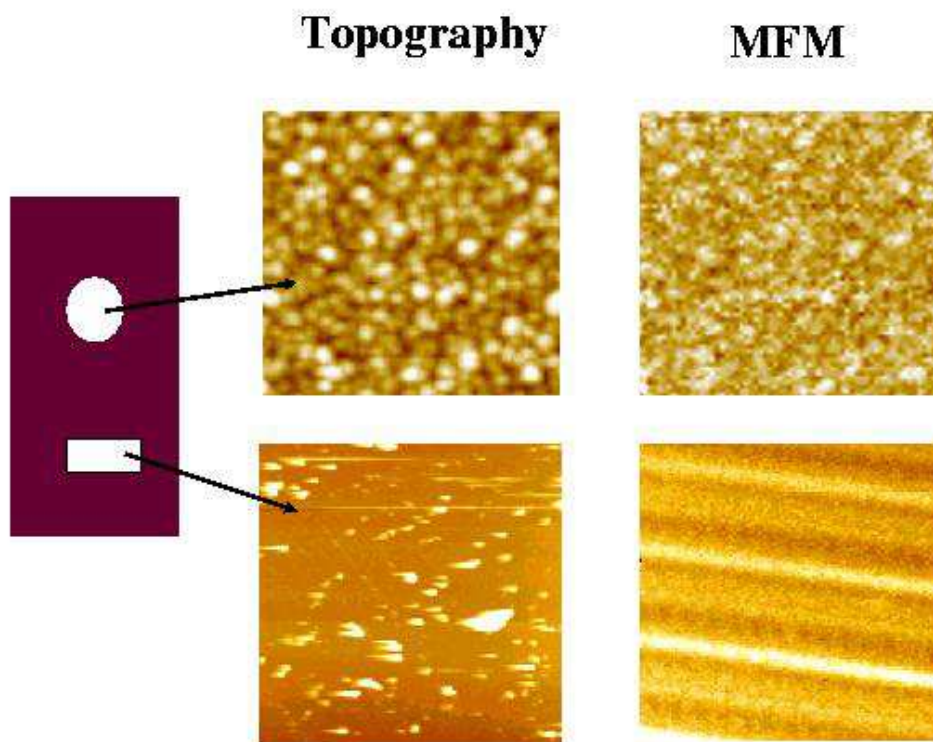


Fig. 13. Left side sketch shows the fullerene film with the two irradiated regions: the upper ellipse corresponds to the laser illuminated region (Makarova, Han, Esquinazi, da Silva, Kopelevich, Zakharova, and Sundqvist, 2003) and the lower rectangle to the region where 20 spots of $1.8 \mu\text{m}$ diameter each were irradiated with a proton microbeam with a current of 500 pA and a fluence between 0.068 and $68 \text{ nC}/\mu\text{m}^2$. In contrast to the spot irradiation in HOPG (see section 3.1.2) no change in the topography has been detected after irradiation of the spots in the fullerene film. All images correspond to an area of $5 \times 5 \mu\text{m}^2$.

well recognizable. In contrast to the laser illumination on C_{60} film and proton irradiation in HOPG, proton irradiation of spots of micrometer size on the fullerene film do not produce appreciable changes in the topography. The magnetic domains are however notable, see Fig. 13.

These results obtained after irradiation of the thin films are unexpected and indicate either the hydrogen concentration in the sample or surrounding before irradiation is relevant and/or the defect concentration in the first micrometer from the sample surface and produced by the proton beam is not negligible. Because the thickness of the film is below $1 \mu\text{m}$ most of the protons go through the material.

4 Annealing and Aging Effects

We have measured with the SQUID some of the proton irradiated samples months after the irradiation. Depending on the sample, the enhancement of the magnetic order decreased or even vanished after more than 8 months leaving them at room temperature and in air. However, the magnetic signal remained for some of them even after one year. The reason for the different behavior is not known yet. In this section we shall summarize results that provide evidence for aging effects in the magnetic ordering, as well as annealing effects at high temperatures, measured by SQUID or MFM. Taking into account previous reports on the behavior and diffusion of hydrogen in graphite (Atsumi, 2002) as well as aging effects at room temperature in the magnetization of the fullerene $C_{60}H_{24}$ (Antonov, Bashkin, Khasanov, Moravsky, Morozov, Shulga, Ossipyan, and Ponyatovsky, 2002) one may expect to observe some time dependence in the magnetic response at the irradiated surface by MFM (or in the bulk magnetic moment by SQUID) if H is involved in the induced magnetism and a diffusion takes place. Two different measurements were done to test the possible influence of H diffusion on the magnetic signals. We measured different irradiated spots on HOPG and irradiated amorphous carbon film just after irradiation and after leaving the samples several months at room temperature. Other samples we annealed at high temperatures in vacuum or He atmosphere.

Figure 14 shows the magnetic moment of a disordered carbon sample before, just after proton irradiation and after one year at room temperature (after irradiation). It is clearly seen that the ferromagnetic-like hysteresis vanishes after one year.

Figures 15(a) and (b) shows the topography (top) and MFM (bottom) images of two spots and their surroundings created with $0.2 \text{ nC}/\mu\text{m}^2$ and $24.5 \text{ nC}/\mu\text{m}^2$ on sample 1. The measurement was done one day after proton irradiation. Line scans of the topography (top) and MFM (bottom) images are shown in Fig. 15(c). As shown in this figure a clear enhancement in both topography and MFM signals at the irradiated region is clearly found. The enhancement of the topographic swelling increases with fluence with our irradiation conditions. For example, the peak height is $\sim 8 \text{ nm}$ ($\sim 225 \text{ nm}$) for a fluence of $0.2 \text{ nC}/\mu\text{m}^2$ ($24.5 \text{ nC}/\mu\text{m}^2$). However, there is no clear correlation between the increase in swelling height measured by AFM and the maximum phase shift change of the MFM signal at the spot within the fluence range used. As shown in Fig. 15(c) bottom, a magnetic structure within the spot produced with $24.5 \text{ nC}/\mu\text{m}^2$ appears, an indication for the existence of magnetic domains within the area of the irradiated spot.

Figure 16 shows the same measurements as in Fig. 15 for the same two spots, but obtained 8 months later. After this time we found clear changes in the to-

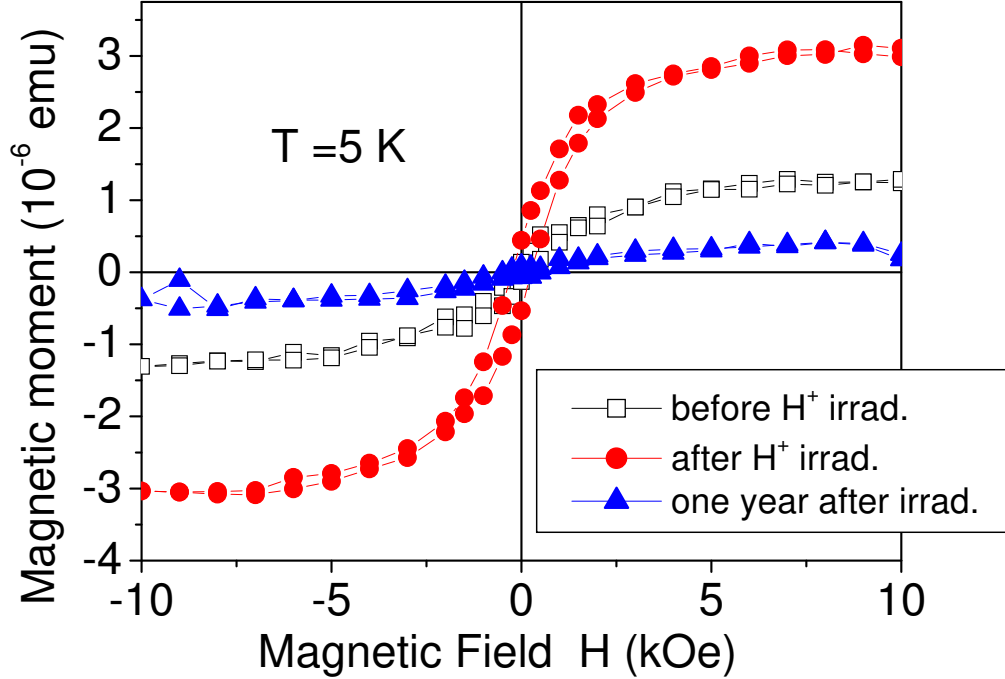


Fig. 14. Magnetic moment (the diamagnetic background was subtracted) as a function of applied field for the disordered carbon film CH577a after preparation by PLD (before irradiation (\square)), after irradiation (\bullet) and one year later, leaving the sample at room temperature (\blacktriangle).

pography and in the phase shift of the MFM signal at and in the surroundings of the original microspots, see Fig. 16. There are three main changes to be noted: (1) The sharply white spots in MFM images (see the bottom Figs. 15(a) and (b)) on the irradiated area changed to black spots (see bottom Figs. 16(a) and (b)) and the maximum value of phase shift changes from $\sim +0.7^\circ$ to $\sim -0.2^\circ$. It means that the direction of magnetization and its magnitude at the spots changed. (2) There appear clear and localized MFM signals besides the original spot signal (black spots in Figs. 16(a) and (b)). We note also that these “mirror” spots for both fluences are not clearly related to the topographic swellings as can be seen by comparing the line scan signals of topography and MFM of both spots (see Fig. 16(c)). There is also a clear change in the topography at the irradiated spots indicating a lattice relaxation. (3) The MFM images reveal that after 8 months there is a change not only at the spot position and its near neighborhood but also at its surroundings. This change is clearly observable in the vicinity of the spot made with a fluence $24.5 \text{ nC}/\mu\text{m}^2$ where a well discernible domain pattern appears, see bottom Fig. 16(b).

Hydrogen desorption in graphite was and still is a matter of research. Depending on the characteristics of the H-trapping this desorption may or may not be accompanied by a lattice change. Therefore, it is not straightforward to

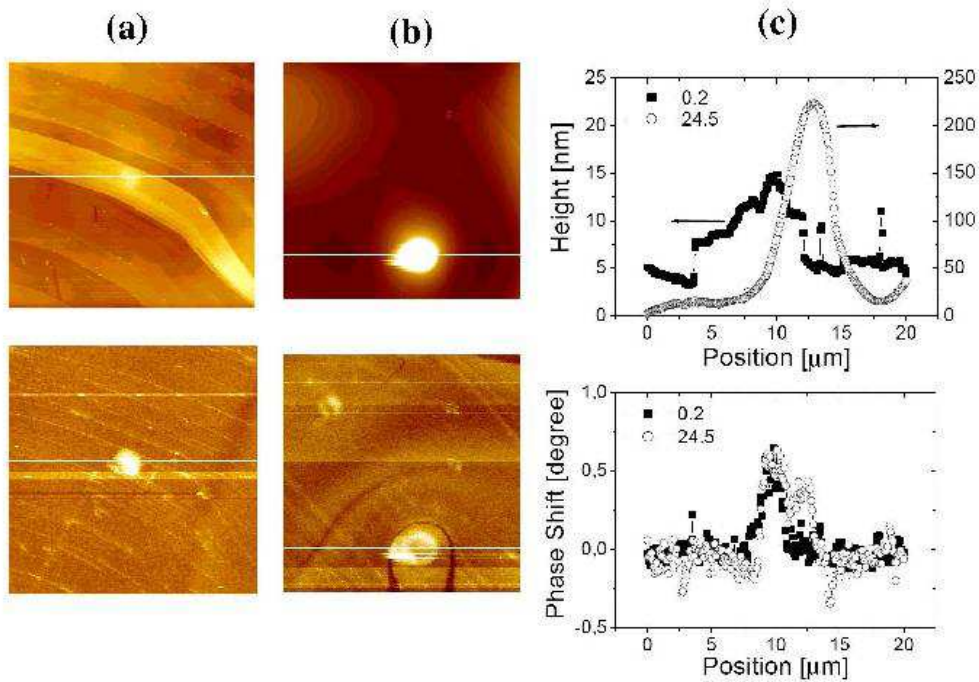


Fig. 15. Topography (top) and MFM (bottom) images ($20 \times 20 \mu\text{m}^2$) of sample 1 for two spots created at $0.2 \text{ nC}/\mu\text{m}^2$ (a) and $24.5 \text{ nC}/\mu\text{m}^2$ (b) and their surroundings measured one day after irradiation. The tip-to-sample distance was 50 nm. (c) Corresponding line scans (white lines in (a) and (b)) of topography (top) and phase shift (bottom) images.

conclude that the aging effects we observed are due only to the H-diffusion without any structural relaxation. Because we got evidence for a structural relaxation, this can influence the effective diffusion of H in the carbon matrix. Therefore, the effective activation energies for H diffusion in our system are not necessarily the same as, for example, those obtained by experimental methods, usually at high temperatures, to study kinetics of diffusion of hydrogen in graphite (Atsumi, 2002).

Certainly, one does not necessarily wait one year to see effects that may be related to hydrogen diffusion. It is quicker to anneal an irradiated sample at high enough temperatures and check for its influence. Figure 17 shows the MFM images obtained for the crosses corresponding to those of Fig. 10(a) and (c) measured at identical conditions after annealing the sample 2 hs at 1000 C in vacuum. Whereas no signal is detected for the cross in (b) ((c) in Fig. 10) magnetic domains are still identified after annealing in the surroundings of the cross (a). Compare this observation to that obtained after aging the spots at room temperature for several months shown in Fig. 16.

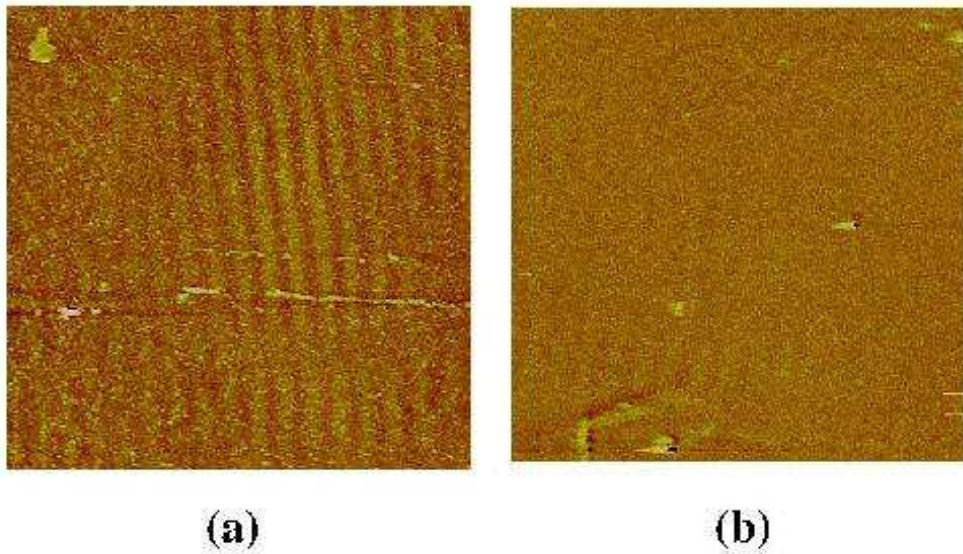


Fig. 17. The figures (a) and (b) show magnetic images of the same crosses shown in Fig. 10(a) and (c) measured under similar conditions with similar MFM tips after annealing them in vacuum at 1000 C for 2 hs. Whereas the crosses are not anymore visible in MFM, domain structure is still detected in (a).

5 Conclusion and Open Issues

In this chapter we have reviewed the main observations after proton irradiation of carbon structures. The main results indicate that proton irradiation can trigger magnetic ordering in graphite. The results after proton irradiation leave no doubt that magnetic ordering exists in a carbon structure without the influence of magnetic ions. Neither the total amount of magnetic impurities is sufficient to account for the measured magnetization nor the creation of magnetic spots in the micrometer range with the proton micro-beam can be understood based on magnetic metal-ion impurity concentration below 1 ppm as the PIXE results indicate. The results obtained up today do indicate that different parameters and sample states may play a role in determining the strength of the induced magnetic ordering. Broad irradiation (i.e. with a proton beam of large diameter) appears to be less effective. The reason for this behavior will be studied in the future, but we speculate that it may be due to the produced defect density. Further experimental characterization (using the broad spectrum of methods in magnetism research) and sample preparation studies are necessary to understand and stabilize the magnetic ordering found in carbon structures. The following issues should be clarified in the near future:

- (1) The role of H-atoms, implanted by irradiation as well as those already in the sample.
- (2) The contribution to the magnetic order from lattice defects produced by irradiation and their possible influence as H-trapping centers.
- (3) Dependence of the magnetic order on the induced type of defect.
- (4) The maximum achievable saturation magnetization in carbon structures.
- (5) The range of Curie temperature.
- (6) Influence of the ion current, fluence and energy of the irradiated particle on the magnetic order.
- (7) Influence of sample temperature.
- (8) Influence of the irradiation angle with respect to the crystallographic *c*-axis of graphite.
- (9) Influence of ion irradiation (other than proton) on the magnetism of carbon structures.
- (10) The effective magnetic moment of magnetic impurities in graphite as well as in disordered carbon structures.

An answer to part of these open questions will take several years of research.

Summarizing briefly recently published theoretical work, which is correlated to the influence of hydrogen in carbon magnetism we note that:

- (1) Hydrogenated nanographite can have a spontaneous magnetization due to

different numbers of mono- and dihydrogenated carbon atoms (Kusakabe and Maruyama, 2003). Theoretical work using local-spin-density approximation calculates the spin polarization of the graphite bands when different atoms as hydrogen, fluor or oxygen are added on a graphene layer and predicts magnetic ordering with fully or partially spin-polarized flat band, upon the added atom (Maruyama and Kusakabe, 2004). Theoretical simulations indicate that a magnetic ordered state should be easier to achieve with a mixture of carbon-hydrogen bonds than fluorinated nanographite (Maruyama, Kusakabe, Tsuneyuki, Akagi, Yoshimoto, and Yamauchi, 2004). Although the calculations were done attaching the hydrogen at the carbon atoms at the edges of a graphene layer, one may speculate that hydrogen can trigger the sp^2 - sp^3 unbalance promoting magnetic ordering in different carbon structures.

- (2) Recently published work indicates that hydrogen modifies substantially the electronic structure of graphite around it. According to STM/AFM measurements (Ruffieux, Gröning, Schwaller, Schlapbach, and Gröning, 2000) a single H-atom interacting with a graphite surface modifies the electronic structure over a distance of 20 to 25 lattice constants.
- (3) Muon spin rotation/relaxation experiments (Chakhalian, Kiefl, Dunsiger, MacFarlane, Miller, and Sonnerup, 2002) indicate that a positive muon in graphite triggers a local magnetic moment around it. Recently published theoretical work (Duplock, Scheffler, and Lindan, 2004) supports this conclusion. It also indicates that upon the type of defect in a graphene layer, hydrogen may not trigger any magnetic ordering.
- (4) The magnetic moment and diffusion of adatom defects in a graphite sheet were studied by Lehtinen, Foster, Ayuela, Krasheninnikov, Nordlund, and Nieminen (2003). The results of a full spin-polarized density functional theory indicate that these defects may have a magnetic moment of about $0.5 \mu_B$. The calculations of Lehtinen, Foster, Ma, Krasheninnikov, and Nieminen (2004) indicate that if an hydrogen encounters an empty vacancy, then it compensates the dangling bond and the magnetic moment of the vacancy vanishes. However, if a vacancy is saturated by an hydrogen atom, a second hydrogen atom will bond to the other side of the vacancy having a magnetic moment of $1.2 \mu_B$ localized on the dangling sp^2 bond.
- (5) New theoretical and experimental work (Chan, Montanari, Gale, Bennington, Taylor, and Harrison, 2004) suggests that hydrogen may play also an important role on the magnetic ordering found in fullerenes.

Acknowledgements

This research is supported by the Deutsche Forschungsgemeinschaft under DFG ES 86/11-1.

References

- Abe, H., Naramoto, H., Iwase, A., Kinoshita, C., 1997. Effect of damage cascades on the irradiation-induced amorphization in graphite. *Nuclear Instruments and Methods in Physics Research B* 127/128, 681–684.
- Antonov, V. E., Bashkin, I. O., Khasanov, S. S., Moravsky, A. P., Morozov, Y. G., Shulga, Y. M., Ossipyan, Y. A., Ponyatovsky, E. G., 2002. Magnetic ordering in hydrofullerite $C_{60}H_{24}$. *J. of Alloys and Compounds* 330-332, 365–368.
- Atsumi, H., 2002. Hydrogen bulk retention in graphite and kinetics of diffusion. *Journal of Nuclear materials* 307-311, 1466–1470.
- Banhart, F., 1999. Irradiation effects in carbon nanostructures. *Rep. Prog. Phys.* 62, 1181–1221.
- Butz, T., Spemann, D., Han, K.-H., Höhne, R., Setzer, A., Esquinazi, P., 2005. The role of nuclear nanoprobe in inducing magnetic ordering in graphite. *Hyperfine Interactions* (in press) .
- Chakhalian, J. A., Kiefl, R. F., Dunsiger, S. R., MacFarlane, W. A., Miller, R., Sonier, J. E., Fischer, J. E., 2002. Evidence for local moment formation around a positive muon in graphite. *Phys. Rev. B* 66, 155107–1–8.
- Chan, J. A., Montanari, B., Gale, J. D., Bennington, S. M., Taylor, J. W., Harrison, N. M., 2004. Magnetic properties of polymerized C_{60} : The influence of defects and hydrogen. *Phys. Rev. B* 70, 041403(R)–1–4.
- Duplock, E. J., Scheffler, M., Lindan, P. J. D., 2004. Hallmark of perfect graphite. *Phys. Rev. Lett.* 92, 225502–1–4.
- Esquinazi, P., Han, K.-H., Höhne, R., Spemann, D., Setzer, A., Butz, T., 2005. Examples of room-temperature magnetic ordering in carbon-based structures. *Phase Transitions* 78, 155–168.
- Esquinazi, P., Setzer, A., Höhne, R., Semmelhack, C., Kopelevich, Y., Spemann, D., Butz, T., Kohlstrunk, B., Lösche, M., 2002. Ferromagnetism in oriented graphite samples. *Phys. Rev. B* 66, 024429–1–10.
- Esquinazi, P., Spemann, D., Höhne, R., Setzer, A., Han, K.-H., Butz, T., 2003. Induced magnetic ordering by proton irradiation in graphite. *Phys. Rev. Lett.* 91, 227201–1–4.
- Estrade-Szwarckopf, H., 2004. XPS photoemission in carbonaceous materials: A “defect” peak beside the graphitic asymmetric peak. *Carbon* 42, 1713–1721.
- Fujita, M., Wakabayashi, K., Nakada, K., Kusakabe, K., 1996. Peculiar localized state at zigzag graphite edge. *J. Phys. Soc. Jpn.* 65, 1920–1923.
- González, J., Guinea, F., Vozmediano, M. A. H., 2001. Electron-electron interactions in graphene sheets. *Phys. Rev. B* 63, 134421–1–8.
- Han, K.-H., Esquinazi, P., 2004. Quantitative determination of the magnetization of proton irradiated spots in graphite with magnetic force microscopy. *J. Appl. Phys.* 96, 1581–1584.
- Han, K.-H., Spemann, D., Esquinazi, P., Höhne, R., Riede, V., Butz, T., 2003a. Ferromagnetic spots in graphite produced by proton irradiation. *Adv. Mater.* 15, 1719–1722.
- Han, K.-H., Spemann, D., Höhne, R., Setzer, A., Makarova, T., Esquinazi, P., Butz, T., 2003c. Addendum. *Carbon* 41, 2425.
- Han, K.-H., Spemann, D., Höhne, R., Setzer, A., Makarova, T., Esquinazi, P., Butz,

- T., 2003b. Observation of intrinsic magnetic domains in C₆₀ polymer. *Carbon* 41, 785–795.
- Höhne, R., Esquinazi, P., Han, K.-H., Spemann, D., Setzer, A., Schaufuß, U., Riede, V., Butz, T., Streubel, P., Hesse, R., 2004. Ferromagnetic structures in graphite and amorphous carbon films produced by high energy proton irradiation. In: Raabe, D. (Ed.), *Proceedings of the 16. International Conference of Soft Magnetic Materials* (ISBN 3-514-00711-X).
- Kelly, B. T., 1981. *Physics of Graphite*. London: Applied Science Publishers.
- Koike, J., Pedraza, D. F., 1994. Dimensional changes in highly oriented pyrolytic graphite due to electron-irradiation. *J. Mater. Res.* 9, 1899–1907.
- Kusakabe, K., Maruyama, M., 2003. Magnetic nanographite. *Phys. Rev. B* 67, 092406–1–4.
- Lehtinen, P. O., Foster, A. S., Ayuela, A., Krasheninnikov, A., Nordlund, K., Nieminen, R. M., 2003. Magnetic properties and diffusion of adatoms on a graphene sheet. *Phys. Rev. Lett.* 91, 017202–1–4.
- Lehtinen, P. O., Foster, A. S., Ma, Y., Krasheninnikov, A., Nieminen, R. M., 2004. Irradiation-induced magnetism in graphite: a density-functional study. *Phys. Rev. Lett.* 93, 187202–1–4.
- Lohau, J., Kirsch, S., Carl, A., Dumpich, G., Wassermann, E., 1999. Quantitative determination of effective dipole and monopole moments of magnetic force microscopy tips. *J. Appl. Phys.* 86, 3410–3417.
- Lohau, J., Kirsch, S., Carl, A., Wassermann, E., 2000. Quantitative determination of the magnetization and stray field of a single domain Co/Pt dot with magnetic force microscopy. *Appl. Phys. Lett.* 76, 3094–3096.
- Makarova, T., Han, K., Esquinazi, P., da Silva, R. R., Kopelevich, Y., Zakharova, I. B., Sundqvist, B., 2003. Magnetism in photopolymerized fullerenes. *Carbon* 41, 1575–1584.
- Makarova, T., 2003. Magnetism of carbon-based materials. Vol. 45 of *Studies of High Temperature Superconductors*. NOVA Science Publishers, Inc., pp. 107–169.
- Maruyama, M., Kusakabe, K., Tsuneyuki, S., Akagi, K., Yoshimoto, Y., Yamauchi, J., 2004. Magnetic properties of nanographite with modified zigzag edges. *J. of Physics and Chemistry of Solids* 65, 119–122.
- Maruyama, M., Kusakabe, K., 2004. Theoretical prediction of synthesis methods to create magnetic nanographite. *J. Phys. Soc. Jpn.* 73, 656–663.
- Murata, K., Ushijima, H., Ueda, H., Kawaguchi, K., 1991. Magnetic properties of amorphous-like carbons prepared by tetraaza compounds by the chemical vapour deposition (CVD) method. *J. Chem. Soc., Chem. Commun.* , 1265–6.
- Murata, K., Ushijima, H., Ueda, H., Kawaguchi, K., 1992. A stable carbon-based organic magnet. *J. Chem. Soc., Chem. Commun.* , 567–569.
- Muto, S., Tanabe, T., 1997. Damage process of electron irradiated graphite studied by transmission electron microscopy: I. High resolution observation of highly graphitized carbon fibre. *Phil. Mag. A* 76, 679–690.
- Niwase, K., 1995. Irradiation-induced amorphization of graphite. *Phys. Rev. B* 52, 15785–98.
- Ovchinnikov, A. A., Shamovsky, I. L., 1991. The structure of ferromagnetic phase of carbon. *J. of Molecular Structure (Theochem)* 251, 133–140.
- Rousseau, B., Estrade-Szwarckopf, H., Thomann, A.-L., Brault, P., 2003. Stable C-

- atom displacements on HOPG surface under plasma low-energy argon ion bombardment. *Appl. Phys. A* 77, 591–598.
- Ruffieux, R., Gröning, O., Schwaller, P., Schlapbach, L., Gröning, P., 2000. Hydrogen atoms cause long-range electronic effects on graphite. *Phys. Rev. Lett.* 84, 4910–4914.
- Schindler, K., Spemann, D., Ziese, M., Diaconu, M., Schmidt, H., Esquinazi, P., Butz, T., 2005. Magnetic crosses produced with a proton microbeam on a graphite surface. To be published .
- Siegele, R., Roth, J., Scherzer, B. M. U., Pennycook, S. J., 1993. Damage and deuterium trapping in highly-oriented pyrolytic graphite. *J. Appl. Phys.* 73, 2225–2233.
- Spemann, D., Han, K.-H., Esquinazi, P., Höhne, R., Butz, T., 2004. Ferromagnetic microstructures in highly oriented pyrolytic graphite created by high energy proton irradiation. *Nuclear Instruments and Methods in Physics Research B* 219-220, 886–890.
- Spemann, D., Han, K.-H., Höhne, R., Makarova, T., Esquinazi, P., Butz, T., 2003. Evidence for intrinsic weak ferromagnetism in a C₆₀ polymer by PIXE and MFM. *Nuclear Instruments and Methods in Physics Research* 210, 531–536.
- Takeuchi, M., Muto, S., Tanabe, T., Arai, S., Kuroyanagi, T., 1997. Damage process of electron irradiated graphite studied by transmission electron microscopy: II. Analysis of extended energy-loss fine structure of highly oriented pyrolytic graphite. *Phil. Mag. A* 76, 691–700.
- Tanabe, T., 1996. Radiation damage of graphite - degradation of material parameters and defect structures. *Phys. Scr.* T64, 7–16.
- Wang, T., Wang, W., Chen, B., 1992. The irradiation effect of MeV protons on diamond-like carbon films. *Nuclear Instruments and Methods in Physics Research B* 71, 186–190.
- Ziegler, J. F., 1977-1985. *The stopping and range of ions in matter*. Pergamon Press, New York.